Javed *et al. Carbon Balance and Management* (2025) 20:9
https://doi.org/10.1186/s13021-025-00300-9

Carbon Balance and Management

RESEARCH Open Access

The influence of agricultural drought on carbon emissions across the four sub-regions of China

Tehseen Javed[1,2,3,4], Zhenhua Wang[1,2,3,4*], Jian Liu[1,2,3,4], Wenhao Li[1,2,3,4], Haixia Lin[1,2,3,4], Pengpeng Chen[1,2,3,4] and Jihong Zhang[1,2,3,4]

Abstract

Vegetation is crucial in carbon sequestration, as it stores soil carbon and biomass. However, agricultural droughts significantly reduce vegetation growth, directly impacting the amount of carbon sequestered through photosynthesis. This study investigates the effects of agricultural drought on carbon emissions across four sub-regions of China, Northwest China, North China, the Qinghai-Tibet region, and South China, from 2001 to 2020. Three remote sensing-based drought indices, the Moisture Anomaly Index (MAI), Vegetation Anomaly Index (VAI), and Temperature Anomaly Index (TAI) were used for drought monitoring. Advanced statistical techniques were employed to explore the relationship between these indices and carbon emissions, including auto-correlation and spatial cross-correlation. The results indicate that temporal variations between carbon emissions and agricultural drought indices exhibit distinct regional patterns. Among the indices, VAI demonstrated the strongest correlation with carbon emissions, with values ranging from $r = 0.56$ to 0.76. Carbon emissions varied significantly across regions, with the highest recorded in North China, followed by South China, Northwest China, and Qinghai-Tibet regions. Spatial cross-correlation analysis revealed that the highest positive correlation ($r > 0.5$) between carbon emissions and drought indices was observed in South China, whereas a moderate correlation was found between MAI and carbon emissions in Northwest China. The correlation between VAI and carbon emissions ranged from r = -0.6 to > 0.8. TAI exhibited a positive correlation with carbon emissions in South China, whereas negative correlations were observed in Northwest China and northeast North China. These findings provide valuable insights for mitigating drought-induced carbon emissions and promoting sustainable land management practices.

Keywords Agricultural drought, Carbon emission, Moisture anomaly index (MAI), Spatial cross-correlation, And promote sustainable land management practices

*Correspondence:
Zhenhua Wang
wzh2002027@163.com
[1]College of Water Conservancy & Architectural Engineering, Shihezi University, Shihezi 832000, Xinjiang, China
[2]Key Laboratory of Modern Water-Saving Irrigation of Xinjiang Production & Construction Group, Shihezi University, Shihezi 832000, Xinjiang, China
[3]Technology Innovation Center for Agricultural Water and Fertilizer Efficiency Equipment of Xinjiang Production & Construction Group, Shihezi University, Shihezi 832000, Xinjiang, China
[4]Engineering Technology Center for Comprehensive Utilization of Saline and Alkaline Land in the Xinjiang Production & Construction Group, Shihezi 832000, Xinjiang, China

Introduction

Agricultural drought, characterized by below-average rainfall, reduces soil moisture, stunted crop growth, and lower farm productivity [1, 2]. These droughts have far-reaching consequences, affecting food security, economic stability, and environmental sustainability [3, 4]. While natural climatic fluctuations contribute to drought conditions, anthropogenic factors such as land-use changes, unsustainable water management, and climate change exacerbate their severity [5, 6]. In China, particularly in northern and western regions, agricultural drought has become increasingly frequent and severe, significantly impacting crop production and water resources [7]. As one of the world's most populous nations, China relies heavily on agriculture for economic and food security, making it highly vulnerable to drought-induced losses. For instance, the 2019 drought in Liaoning province caused agricultural losses exceeding 1.1 billion USD, affecting more than 2.8 million people [8, 9].

To monitor and assess agricultural drought, remote sensing-based indices such as the Normalized Difference Vegetation Index (NDVI), Enhanced Vegetation Index (EVI), and Vegetation Condition Index (VCI) have been widely adopted [10–12]. These indices help evaluate vegetation health, soil moisture status, and drought severity [13]. NDVI, for example, assesses the difference in reflectance between near-infrared and red light, indicating vegetation density and photosynthetic activity. EVI improves upon NDVI by reducing atmospheric interference and enhancing sensitivity to vegetation cover changes, while VCI quantifies deviations in vegetation health from long-term norms, offering critical insights into drought impacts [14–16]. These indices are instrumental in guiding agricultural policies, water resource management, and land-use planning, making them essential tools for mitigating drought risks [17, 18].

Beyond agricultural productivity, droughts significantly affect carbon emissions and climate change. Agricultural drought reduces vegetation cover, limiting carbon sequestration while increasing carbon release from soil and decaying biomass [8, 18]. Prolonged drought conditions intensify soil erosion and microbial activity, accelerating the decomposition of organic matter and releasing stored carbon into the atmosphere [19, 20]. Furthermore, the reliance on energy-intensive irrigation practices during drought increases greenhouse gas emissions [3, 8, 21]. The cyclical nature of this interaction, where carbon emissions drive climate change, exacerbating drought conditions, creates a feedback loop that intensifies environmental challenges [15, 21–23].

While previous research has explored the correlation between agricultural drought and carbon emissions, several gaps remain [22, 24, 25]. Many studies have relied on singular indices or models, failing to capture the complexity of regional variations and the interplay between environmental factors [3, 23, 26, 27]. Furthermore, existing studies often lack comprehensive spatial analyses that account for heterogeneity in drought impacts and carbon fluxes [3, 20, 26]. The interactive mechanisms through which drought influences carbon dynamics, such as changes in vegetation stress, soil moisture depletion, and land-use alterations, have also been inadequately examined [21, 28]. Although studies like Liu et al. (2014) [19] and Wolf et al. (2023) [27] have identified drought-induced carbon losses in specific regions, they have not fully addressed the underlying drivers or the broader implications for global carbon cycles [19, 27]. The novelty of this study lies in its integrated, multi-model approach, which combines advanced remote sensing techniques, spatial analysis, and machine learning to comprehensively assess the relationship between agricultural drought and carbon emissions. Unlike previous studies focusing on isolated factors, our research incorporates diverse datasets and considers spatial heterogeneity, allowing for a more nuanced understanding of drought-induced carbon fluxes. Additionally, we analyze drought impacts across varied environmental conditions, providing insights applicable to regional and global contexts. By bridging the gaps in current research, this study offers a deeper understanding of the mechanisms linking agricultural drought and carbon emissions, ultimately informing more effective mitigation strategies for climate resilience and sustainable land management.

This study was initiated to address these shortcomings, with a clear goal of (1) exploring the spatial and temporal variations in agricultural drought indices and carbon emissions from 2001 to 2020 across China's four subregions and (2) identifying the link between agricultural drought indices and carbon emissions during periods of extreme drought and wet years. The findings of this study are expected to enhance understanding of how agricultural droughts affect carbon emissions, paving the way for developing strategies to lessen the impact of agricultural droughts on carbon emissions and to foster sustainable land management techniques.

Study area

China has significant differences in climate and ecological conditions [29]. Consequently, the research area divided its focus into four distinct geographical zones: Northwest China, North China, the Qinghai-Tibet area, and South China [30]. Northwest China experiences arid and semi-arid conditions with scarce water availability, while a temperate continental climate characterizes North China. On the other hand, the Qinghai-Tibet region is known for its high elevation and alpine climate [31]. In contrast, South China enjoys a subtropical climate with more abundant rainfall [7]. These climatic

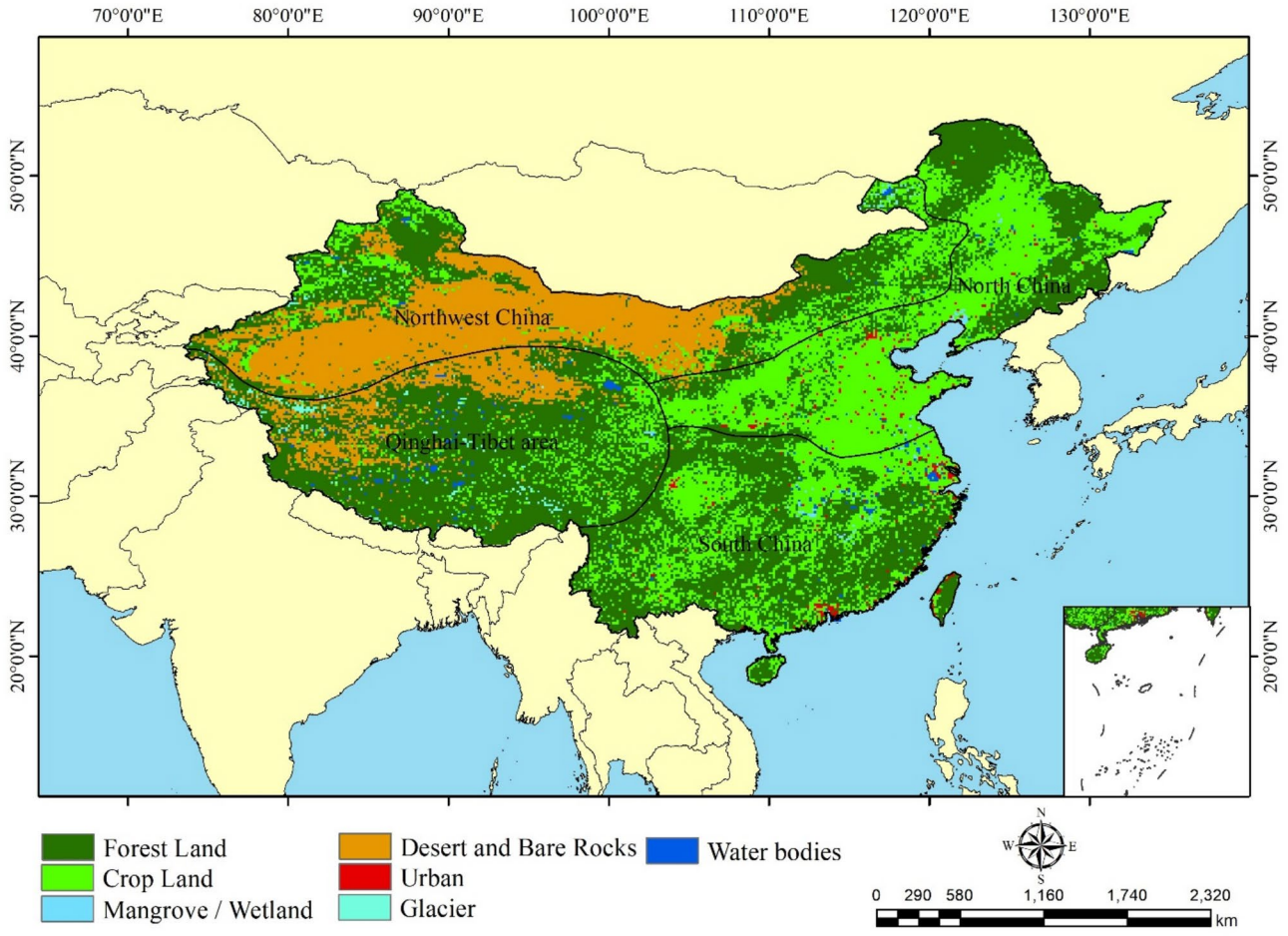

Fig. 1 Map of study area

Table 1 Showing data sources

Data	Resolution	Data Source	Role
GLASS SM	Daily Global 1-km	http://glass.umd.edu/soil_moisture/	Soil moisture
MOD13Q1	16-Day Global 250 m	http://earthexplorer.usgs.gov	Vegetation Indices
MOD11C2	8-Day Global 0.05°	http://earthexplorer.usgs.gov	Land Surface Temperature
NBS	Monthly	https://www.ceads.net/	CO_2 emissions

differences significantly affect farming methods and the carbon cycle.

Moreover, the vegetation and land use in these sub-regions vary. The Qinghai-Tibet area primarily features grasslands and alpine ecosystems, whereas North and South China are marked by various agricultural landscapes [16]. The vegetation type and land use are crucial in carbon cycling and emissions. Each area has its capacity for carbon storage, whether through natural vegetation or agricultural activities [32]. Assessing carbon sequestration capabilities across different ecosystems is vital for creating practical mitigation approaches. An understanding of how agricultural drought affects carbon cycling in China can be gained by analyzing and comparing these sub-regions.

The land use information in Fig. 1 was obtained from the Global Land Cover Data (GLCNMO, version 3) provided by the National Mapping Organization. The dataset, with a 500 m grid size, follows the FAO's Land Cover Classification System and has been validated by the European Space Agency's Climate Change Initiative.

Data and methods

Remote sensing datasets

This research employed datasets including MODIS NDVI, LST, GLASS SM, and CO_2 emissions within the study area.

Soil moisture

A comprehensive soil moisture product, GLASS SM, offering a global resolution of 1 km and daily spatiotemporal continuity, was utilized to determine soil moisture levels from 2000 to 2020. The creation of GLASS SM involved integrating various datasets, such as albedo, land surface temperature, and leaf area index from the Global Land Surface Satellite (GLASS) suite. Additionally, it incorporated the European reanalysis (ERA5-Land) soil moisture product, ground-based measurements from the International Soil Moisture Network (ISMN), and supplementary data sources, including MERIT DEM and the Global gridded soil information (SoilGrids). This product quantifies explicitly the volumetric water content in the top 0–5 cm of soil.

MODIS normalized difference vegetation index (NDVI)

The MODIS NDVI (MOD13Q1, Collection 6) was obtained from (http://earthexplorer.usgs.gov), with a temporal and spatial resolution of 16 days and 250 m, respectively [33]. Further, 16 days of free NDVI pixel composites were used for the entire period from 2000 to 2021. These 16 days of data averaged for the monthly time step.

MODIS land surface temperature (LST)

Version 6 of the MOD11C2 product offers a Land Surface Temperature and Emissivity series, which can be accessed from (http://earthexplorer.usgs.gov). This da taset features a spatial and temporal resolution of 0.05 degrees and eight days. The product consists of 17 layers with day and nighttime observation. For quality control assessments, the number of clear-sky observations, the percentage of land in the grid, and emissivity from bands 20, 22, 23, 31, and 32.

Carbon emissions data

Data on carbon emissions was sourced from the China Carbon Accounting Database, accessible at (https://www.ceads.net/), and the National Bureau of Statistics of China (NBS). Furthermore, this data was utilized to predict carbon emissions. The following formula was used to calculate carbon emissions.

$$CO_{2i} = \sum_{i=1}^{n} \sum_{j=1}^{t} (E_{ij} \times LCV_{ij} \times CC_{ij} \times COF_{ij}) \quad (1)$$

In this context, 'CO_{2i}' represents the carbon emissions for each sub-regional unit or province *'i'*. The variable '*n*' represents the total number of provinces under consideration, while 't' signifies the analyzed energy sources. 'Eij' refers to the specific type of energy used in province *'i'*. 'LCV*ij*' indicates the low calorific value of the *'jth'* type of energy consumed in province *'i'*. 'CC_{ij}' is the carbon content in the *'jth'* type of energy usage for province *'i'*, and 'COF*ij*' denotes the oxygen content in the '*jth*' energy type utilized in the same province.

Methods

Standardized anomalies

Standardized anomalies, often called z-scores or standardized deviations, represent a statistical metric that indicates the extent of deviation of a specific data point from the average of a dataset, measured in units of standard deviations. This calculation method is widely applied in diverse disciplines such as climate science, meteorology, and economics. The formula for determining the standardized anomaly (ZA) can be described as follows:

$$ZA_{x,y,t} = \frac{(X_{x,y,t} - \mu_{x,y})}{\sigma_{x,y}} \quad (2)$$

In this context, $ZA_{(x, y,t)}$ represents the Moisture Anomaly Index (MAI), Vegetation Anomaly Index (VAI), or Temperature Anomaly Index (TAI) for the current value at coordinates (x, y) and time t. The symbol $\mu_{(x, y)}$ denotes the average of the reference field, computed at the exact location across a similar period over multiple years. The term $\sigma_{x, y}$ refers to the standard deviation of this reference field. The resulting standardized anomaly (ZA) will be a dimensionless value representing how many standard deviations the data point (X) is away from the mean of the dataset. A positive ZA indicates that the data point is above the mean, while a negative ZA demonstrates that it is below the mean.

Statistical analysis

A measurement known as cross-correlation examines how two or more sets of time series data change over time concerning one another [34]. It is used to assess how well different time series match one another objectively and to pinpoint the precise moment the best match takes place when comparing various time series. The cross-correlation values lie between the negative and positive. A negative correlation links two variables where one variable rises as the other falls and vice versa [6]. In statistics, a correlation coefficient of -1.0 signifies a flawless negative correlation, whereas a coefficient of 0 implies no correlation. Conversely, a coefficient of + 1.0 indicates a flawless positive correlation. When there is a complete negative correlation, it suggests that the two variables in question consistently demonstrate an exact inverse relationship [35].

When two variables consistently show movement in the same direction, this indicates a positive correlation. For instance, if one variable increases and the other also rises or decreases, and the other follows suit, it suggests a

positive link between them. This parallel movement often implies that the same external factors influence both variables, leading to synchronized behavior [34]. In the current study, spatial cross-correlation was used. Spatial cross-correlation analysis can uncover the causal relationship between variables X and Y. Spatial cross-correlation was computed using the following equations.

$$X = [x_1 x_2 \ldots\ldots \chi_n]^T, Y = [y_1 y_2 \ldots\ldots y_n]^T \tag{3}$$

where the letter "T" stands for transposition and 'x_i' and 'y_i' represent the two different measurements of the size for each ith element, where '*i*' ranges from 1 to n."

The centralized variables can be calculated by.

$$X_e = X - \mu_x, Y_e = Y - \mu_y, \tag{4}$$

where μ_x and μ_y indicate the variables' average values, which are written as, respectively, x_i and y_i.

$$\mu_x = \frac{1}{n}\sum_{i=1}^{n} x_i, \mu_y = \frac{1}{n}\sum_{i=1}^{n} y_i \tag{5}$$

The population variances of the two variables are as follows:

$$\begin{array}{l} \sigma_x^2 \\ = \frac{1}{n}\sum_{i=1}^{n}(x_i - \mu_x)^2 \\ = \frac{1}{n}X_e^T X_e, \sigma_y^2 \\ = \frac{1}{n}\sum_{i=1}^{n}(y_i - \mu_y)^2 \\ = \frac{1}{n}Y_e^T Y_e, \end{array} \tag{6}$$

Therefore, 'σ_x' and 'σ_y' denote the standard deviations of the population for 'x_i' and 'y_i,' respectively. Similarly, one can generate a pair of standardized vectors by scaling the centered variables.

$$\chi = \frac{X - \mu_x}{\sigma_x} = \frac{X_e}{\sigma_x}, y = \frac{Y - \mu_y}{\sigma_y} = \frac{Y_e}{\sigma_y}, \tag{7}$$

what statisticians refer to as "standard scores." The lengths of the two vectors, x and y, and their dimensions or the number of system members, n, may be demonstrated to be identical. That is known as the norm of $\|x\|$ and $\|y\|$. As a result,

$$||x|| = x^T x = n, ||y|| = y^T y = n \tag{8}$$

The foundational theories of spatial correlation, including auto-correlation and cross-correlation, hinge on spatial proximity or distance concepts. One can construct an n-by-n unitary spatial weights matrix in this framework as follows.

$$W = [W_{ij}]_{n\times n} \tag{9}$$

This matrix is known as the Unitized Spatial Weights Matrix (USWM). It exhibits three distinct characteristics, which can be derived from a Spatial Contiguity Matrix (SCM): (1) Symmetrical nature, meaning that w_{ij} equals w_{ji}; (2) Diagonal elements are zero, represented by$|w_{ii}| = 0$, indicating that all diagonal entries are zeros; (3) A requirement for unitization, which implies….

$$\sum_{i=1}^{n}\sum_{j=1}^{n} w_{ij} = 1 \tag{10}$$

As a result, a novel metric for spatial cross-correlation analysis can be established, drawing parallels to the improved version of Moran's Index used for spatial auto-correlation. This new measurement is outlined as follows:

$$R_c = x^T W y \tag{11}$$

The spatial cross-correlation index, often Rc, stands for the spatial cross-correlation coefficient (SCI). The SCI, which has a value between – 1 and 1, can be used to demonstrate that a relationship exists. Transposing Rc results in another expression due to the spatial weights matrix's symmetry.

$$R_c = (x^t W y)^T = y^T W^T x = y^T W x \tag{12}$$

which has the same value as Eq in numbers (6). We can construct several models for various applications of spatial analysis from Eqs. (9) and (10), as shown in the above section.

Results

Temporal variations

Figure 2 illustrates the changes over time in agricultural drought indices, precisely, the Moisture Anomaly Index (MAI), Vegetation Anomaly Index (VAI), and Temperature Anomaly Index (TAI), as well as carbon emissions in various sub-regions from 2001 to 2020. Generally, the MAI bar and VAI curves show a consistent pattern. In comparison, TAI with MAI or VAI shows a slightly different pattern. For example, in the northwestern region of China, periods of drought and significant wet, as indicated by values ranging from – 2 to 2 in metrics such as MAI, VAI, and TAI, were recorded in 2001, 2004, 2011, and 2017. The wet events occurred from 2006 to 2007 and 2015 to 2016.

Similarly, prolonged drought events occurred in North China from 2001 to 2003 and 2009 to 2011. Similarly to Northwest China and the Qinghai-Tibet area in North China, persistent wet events occurred from 2014 to 2017. The temporal variations exposed the notable drought and

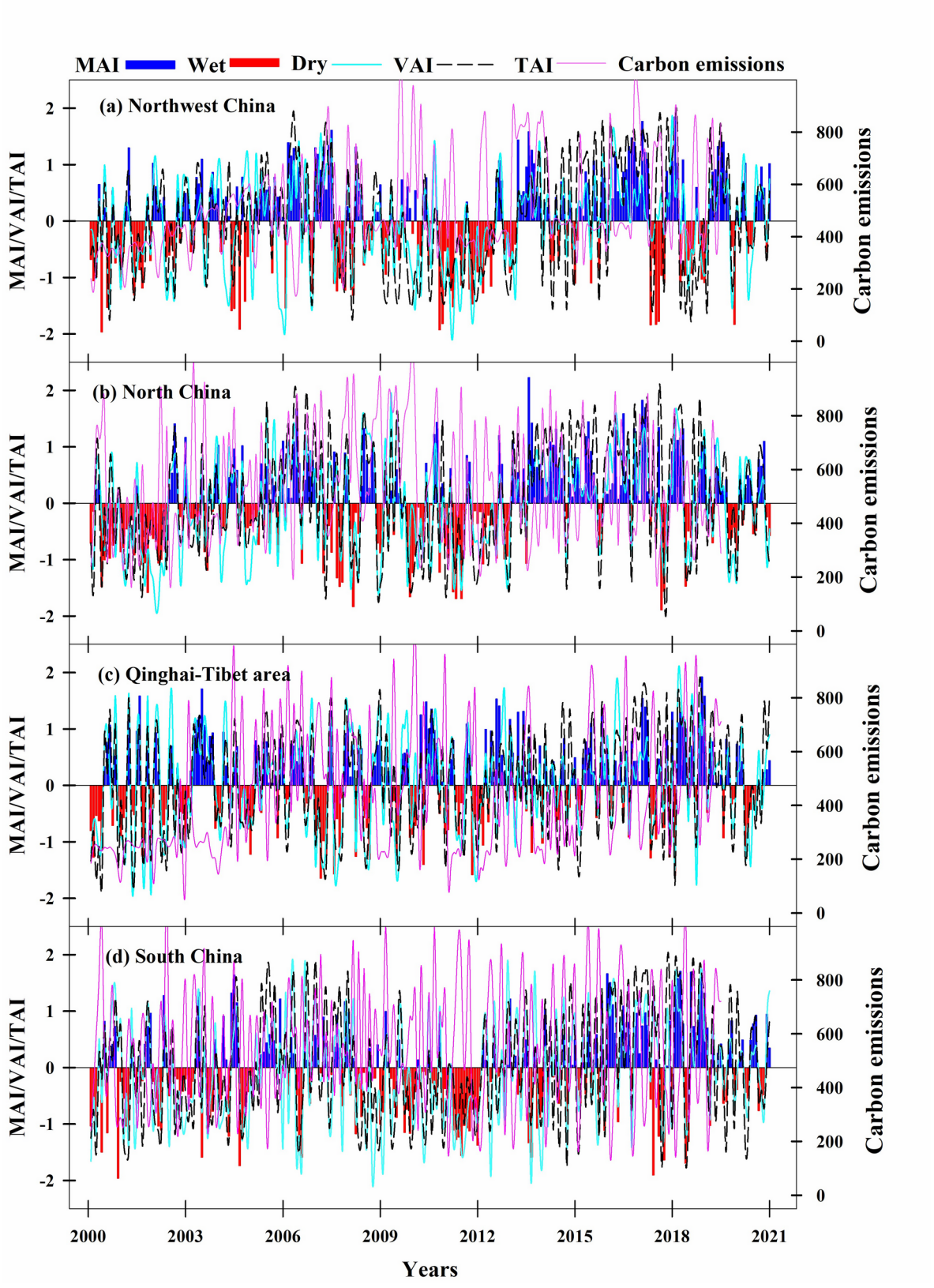

Fig. 2 Temporal distribution of agricultural drought indices and carbon emissions

wet events in 2001, 2004, 2011, and 2017 across all sub-regions. The temporal variation of the carbon emissions exposed that agricultural drought conditions partially impact carbon emissions. For example, in the Northwest drought year 2011, the carbon emissions value reached 800 (Million Tons), while in the drought year 2001, the carbon value was 231(Million Tons).

Similarly, in the North China drought spell 2003, the carbon emissions value was low, and the carbon values were high for the rest of the drought years. On the other hand, in extremely wet years, the emissions are low compared to normal years. For example, in the Qinghai-Tibet area in the extreme wet years 2004 and 2017, lower carbon values of 189 and 211 million tons were observed. Generally, the highest carbon emissions values were obtained in South China.

Spatial correlation analysis

Furthermore, the spatial correlation was performed between three couples of variables, Carbon emission/MAI, or VAI, and/or TAI, for four different seasons across the four different sub-regions (Figs. 3 and 4). In the winter, the correction between carbon emission/MAI or VAI and/or TAI ranged from −0.72 to 0.78, respectively. The correlation between MAI and carbon emission is the highest in January in North China and the lowest in January and February in South China. In February, the Qinghai-Tibet area obtained a negative between MAI and carbon emission. The correlation between the VAI and carbon emission was mainly negative in the winter season, while a positive correlation was obtained in December in Northwest and North China. Generally, the correlation between the TAI and carbon emission is negative. However, a positive correlation was obtained in December between South China and a small area of North China.

Figure 5 illustrates the relationship between indices measuring agricultural drought and carbon emissions during spring across four distinct sub-regions in China. A positive correlation between the MAI and carbon emissions was obtained across North and South China. In the Qinghai-Tibet region and Northwest China, a negative correlation was observed. The correlation between the VAI and carbon emission in South China and Qinghai-Tibet area's two-thirds area had a negative correlation in March and May, while in April, the one-third area had a negative correlation. On the other hand, when correlating the TAI and carbon emissions, a negative correlation was obtained across all sub-regions during March, except a small area of North China.

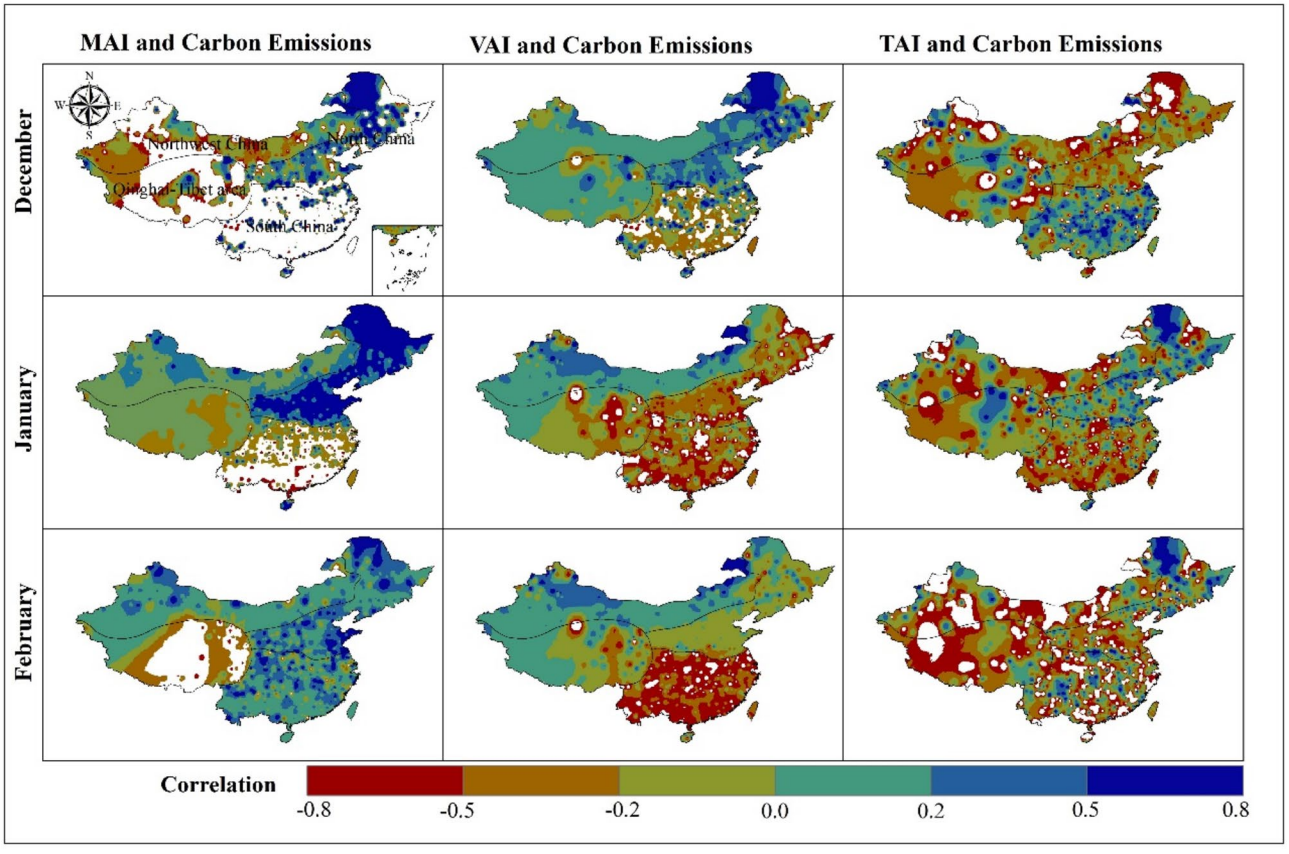

Fig. 3 Correlation between agricultural drought indices and carbon emissions in the winter season

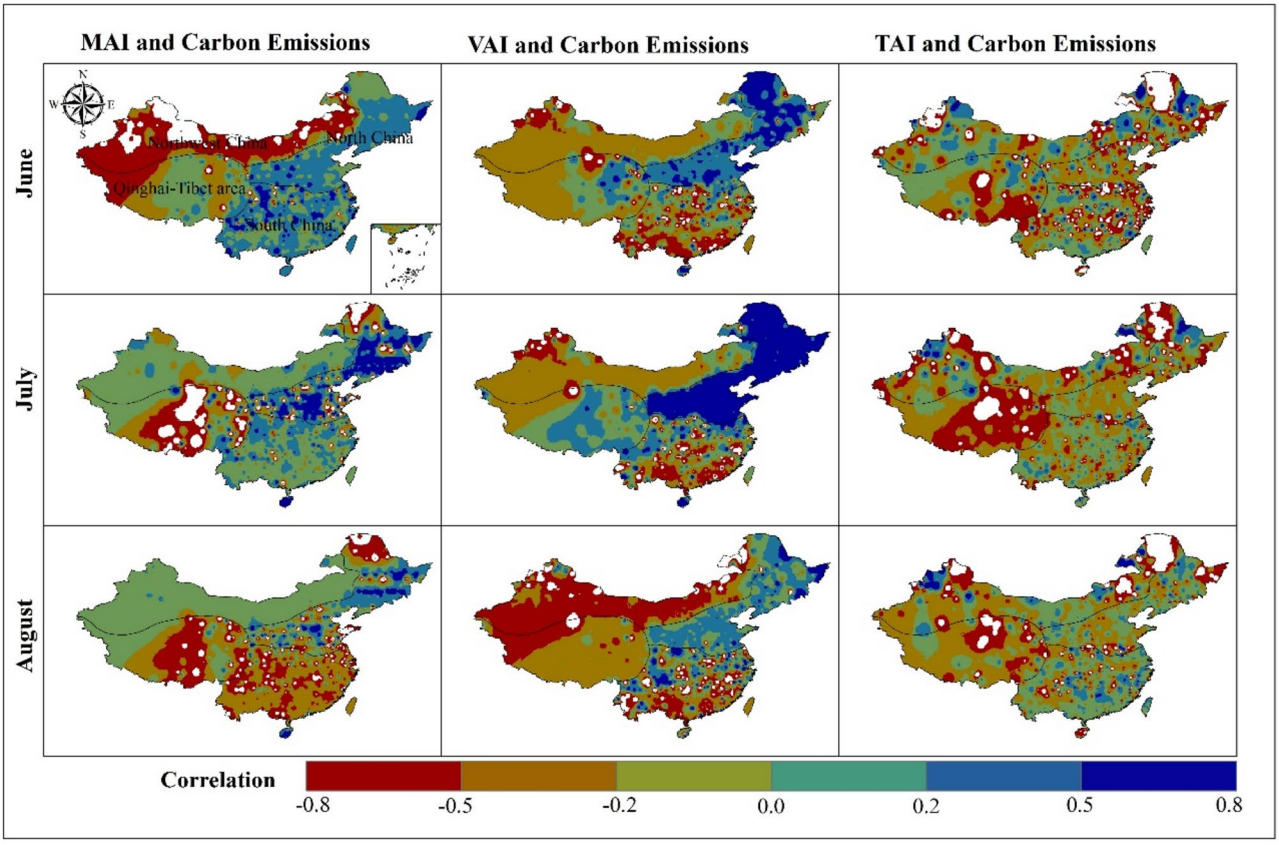

Fig. 4 Correlation between agricultural drought indices and carbon emissions in the summer season

A notable finding was observed when MAI correlates with carbon emissions in the summer season (Fig. 4). For example, a negative correlation was observed across Northwest China in June, while a positive correlation was observed in North and South China. On the other hand, in August, a negative correlation was obtained between North and South China, and a positive correlation was obtained between Northwest China. That finding is reasonable because most North and South China areas are irrigated, and heavy monsoon rain enhances the moisture level in August. Further, when we correlate the carbon emission with VAI, a significantly higher correlation was obtained in North China, followed by the Qinghai-Tibet area. In contrast, a negative correlation was observed in Northwest and South China. The correlation between carbon emission and TAI during the summer season was observed over a majority of the study area.

Figure 6 shows the correlation between carbon emission and agricultural drought indices during autumn. In September and November in North and South China, MAI and carbon emission show a positive correlation $r = > 0.5$. The carbon emission shows an almost negative correlation with VAI over South China. In contrast, the rest of the study shows negative and positive correlations. Additionally, a strong positive correlation between the TAI and carbon emissions ($r = 0.76$) was noted in a limited area of North China in September, whereas a pronounced negative correlation (r = -0.69) was observed in the Qinghai-Tibet area in October. Extreme climate conditions like drought and flood may harm net carbon uptake by restricting photosynthesis and/or boosting soil respiration and litter decomposition. To better understand, the current study examines the effect of agricultural drought and wet conditions on carbon emissions.

Description of carbon emissions in extremely dry and wet years

Figure 7 displays the geographical patterns of carbon emissions across all sub-regions during drought years (2001 and 2011) and wet years (2004 and 2017). Carbon emission shows significant regional differences. For example, in 2001, in North China, the average emission was 365 million tons, while in South China, it was 314 million tons. North China's highest emission was observed, followed by South China, Northwest China, and the Qinghai-Tibet region. These findings indicate high carbon emissions in North and South China's major agricultural and critical manufacturing hubs. Therefore, we further correlate the carbon emission with the drought indicator.

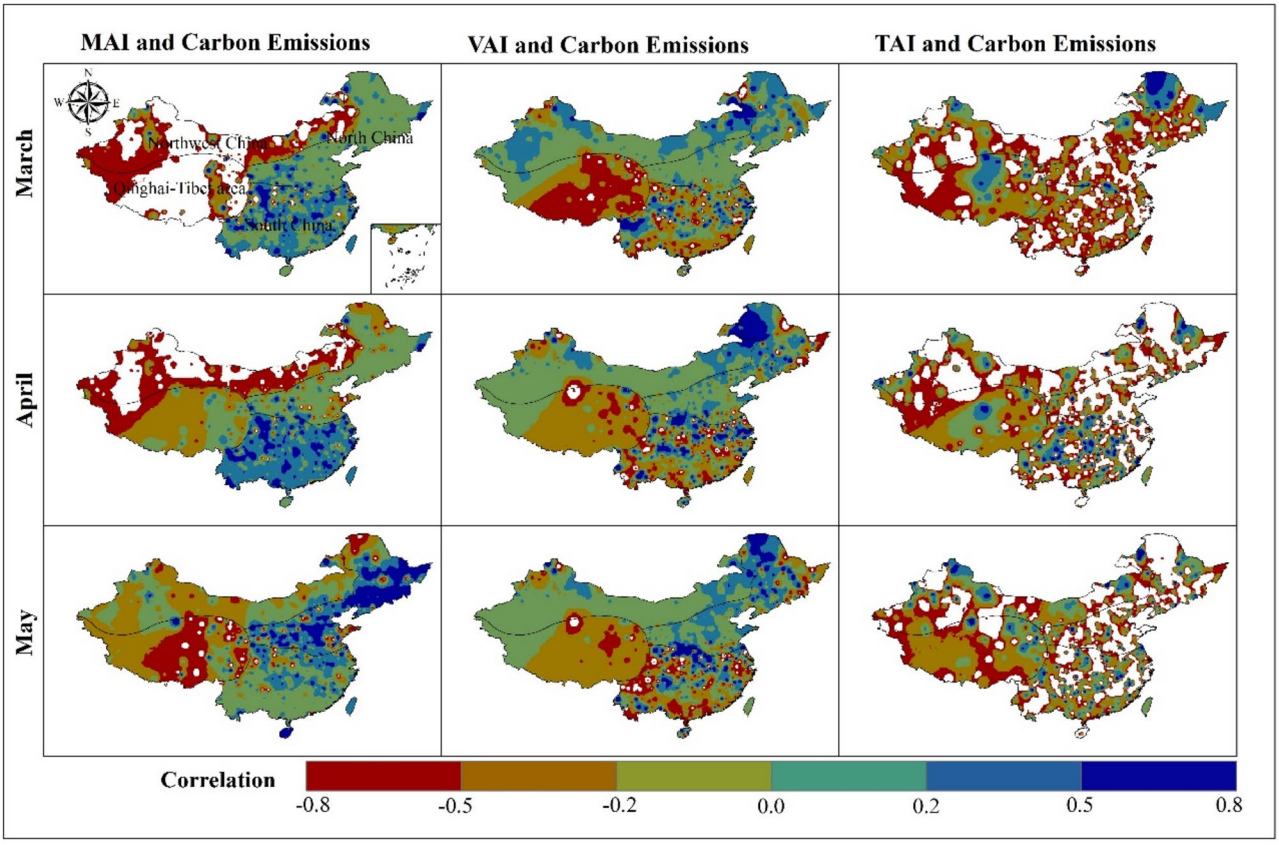

Fig. 5 Correlation between agricultural drought indices and carbon emissions in the spring season

Spatial cross-correlation between the carbon emissions and agricultural drought indices extreme dry and wet years

Figure 8 illustrates the spatial cross-correlation between carbon emissions and MAI. A negative correlation was observed in the Northwest and a small area of North China. In comparison, the highest positive > 0.8 correlation was obtained in South China. The finding is reasonable because, in South China, commonly irrigated agriculture enhances soil moisture and fully utilizes carbon oxides. On the other hand, in Northwest China, during the dry season, soil moisture decreases while vegetation does not fully utilize carbon oxides; therefore, there is a negative correlation.

The correlation between VAI and carbon emission illustrations is in Fig. 9. Overall, the correlation values ranged between − 0.5 to > 0.8. During the drought year 2001, a positive correlation > 0.5 was obtained in South China, the Qinghai-Tibet area, and North China. At the same time, Northwest China's one-third area obtained a negative correlation. In the wet year 2004, the two-third study area shows a positive correlation. Generally, a high positive > 0.5 correlation is observed in South-North China and the Qinghai-Tibet area, and a negative correlation was obtained in Northwest China. That is sound because healthy vegetation uptakes more carbon dioxide. In South and North China, most vegetation is healthy compared to Northwest China.

Generally, a positive correlation was observed in South China, and a negative correlation was obtained in Northwest China and northeast North China during all drought and wet years (Fig. 10). That is logical; in the case of South China, if the plant absorbs more carbon dioxide (CO_2) during photosynthesis, less CO_2 remains trapped in the atmosphere, which can increase the temperatures. Meanwhile, the typical temperature is low in Northwest China and northeast North China, and vegetation does not correctly utilize CO_2.

Discussion

Spatial and temporal variations

Temporal variations of agricultural drought indices, Moisture Anomaly Index (MAI), and Vegetation Anomaly Index (VAI) show a similar pattern across the different sub-regions from 2001 to 2020. Meanwhile, the Temperature Anomaly Index (TAI) with MAI or VAI shows a slightly different pattern. The findings are logical MAI and VAI are closely related to each other because vegetation growth is directly dependent on soil moisture, so when there is a shortage of water, vegetation health is

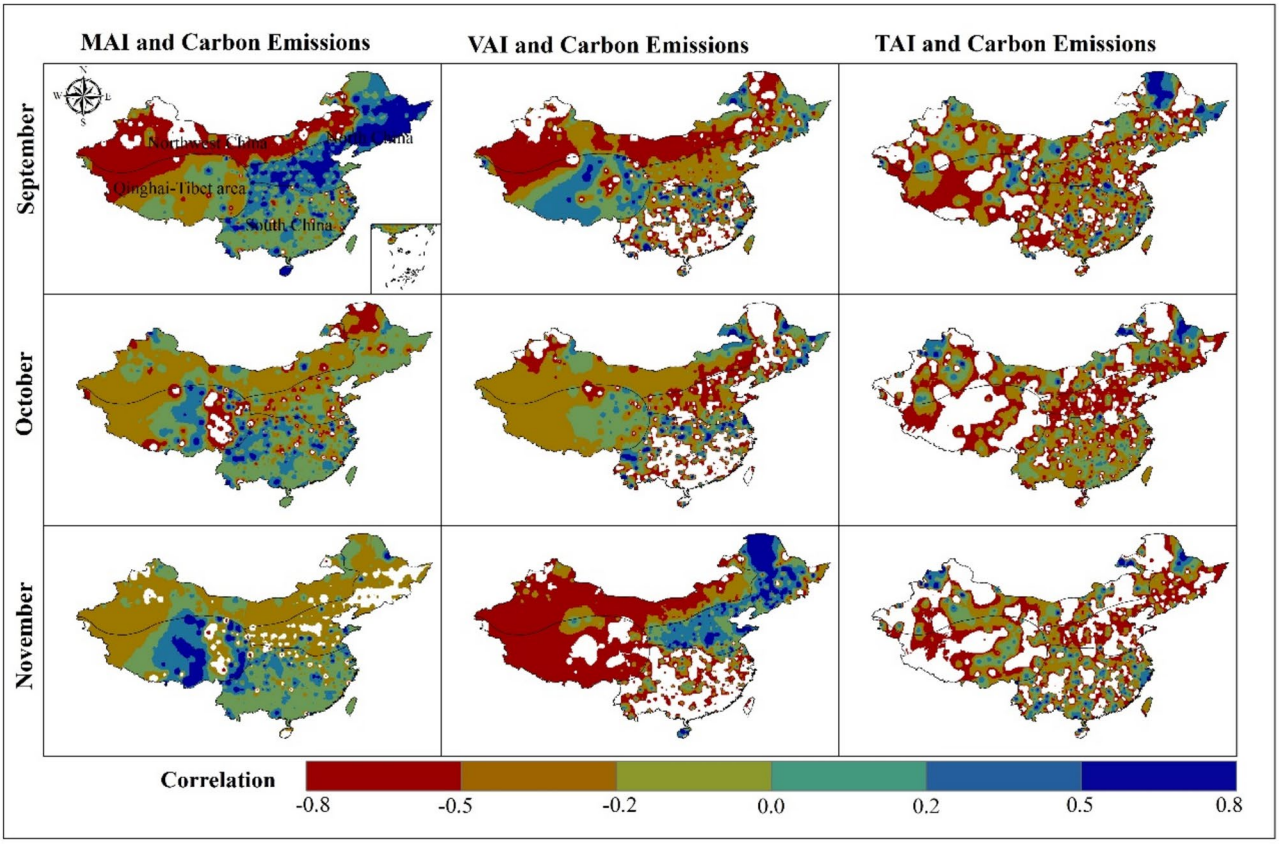

Fig. 6 Correlation between agricultural drought indices and carbon emissions in the autumn season

also affected. This means that changes in moisture availability can significantly impact vegetation growth, and as a result, MAI and VAI will show similar temporal patterns. On the other hand, TAI is related to temperature, which can have a different effect on soil moisture and vegetation growth [36, 37]. Thus, temperature changes may not always be synchronized with changes in moisture availability, leading to differences in the patterns of TAI with MAI or VAI [38].

Our results revealed that temporal variation of carbon emissions shows partial interaction with agricultural drought indices. However, the VAI shows a relatively high correlation with carbon emissions. The findings are logical because, during a drought, plants may close their stomata (pores on their leaves) to conserve water. This closure limits the uptake of carbon dioxide necessary for photosynthesis, leading to reduced photosynthetic activity [16, 39]. As a result, the plant's ability to convert atmospheric carbon dioxide into organic carbon through photosynthesis is diminished [28].

On the other hand, drought stress can lead to increased plant respiration rates. When plants experience water stress, they may respire more to maintain their cellular functions, which can release stored carbon back into the atmosphere as carbon dioxide. Alternatively, it may be due to other factors; the soil is home to 80% of the terrestrial carbon, and the study postulates that under conditions of drought and soil surface cracking or desiccation, this carbon is exposed to oxidation, thereby increasing the carbon dioxide emitted into the atmosphere [40].

Relationship between carbon emissions and agricultural drought indices in extremely dry and wet years

Our result exposed significant regional differences across all sub-regions. South and North China have the highest emissions compared to the Qinghai-Tibet area and Northwest China. South and North China are more industrialized, with higher manufacturing, energy production, and transportation levels than the Qinghai-Tibet area and Northwest China. This industrialization leads to higher carbon emissions, as industries and transportation rely heavily on fossil fuels that emit greenhouse gases, including carbon dioxide [20]. Furthermore, South and North China have much higher population densities than the Qinghai-Tibet area and Northwest China. This higher population density means more people using energy, transportation, and other resources, which leads to higher carbon emissions. Qinghai-Tibet and Northwest China have more extensive grassland areas, which admit carbon dioxide through photosynthesis. In contrast,

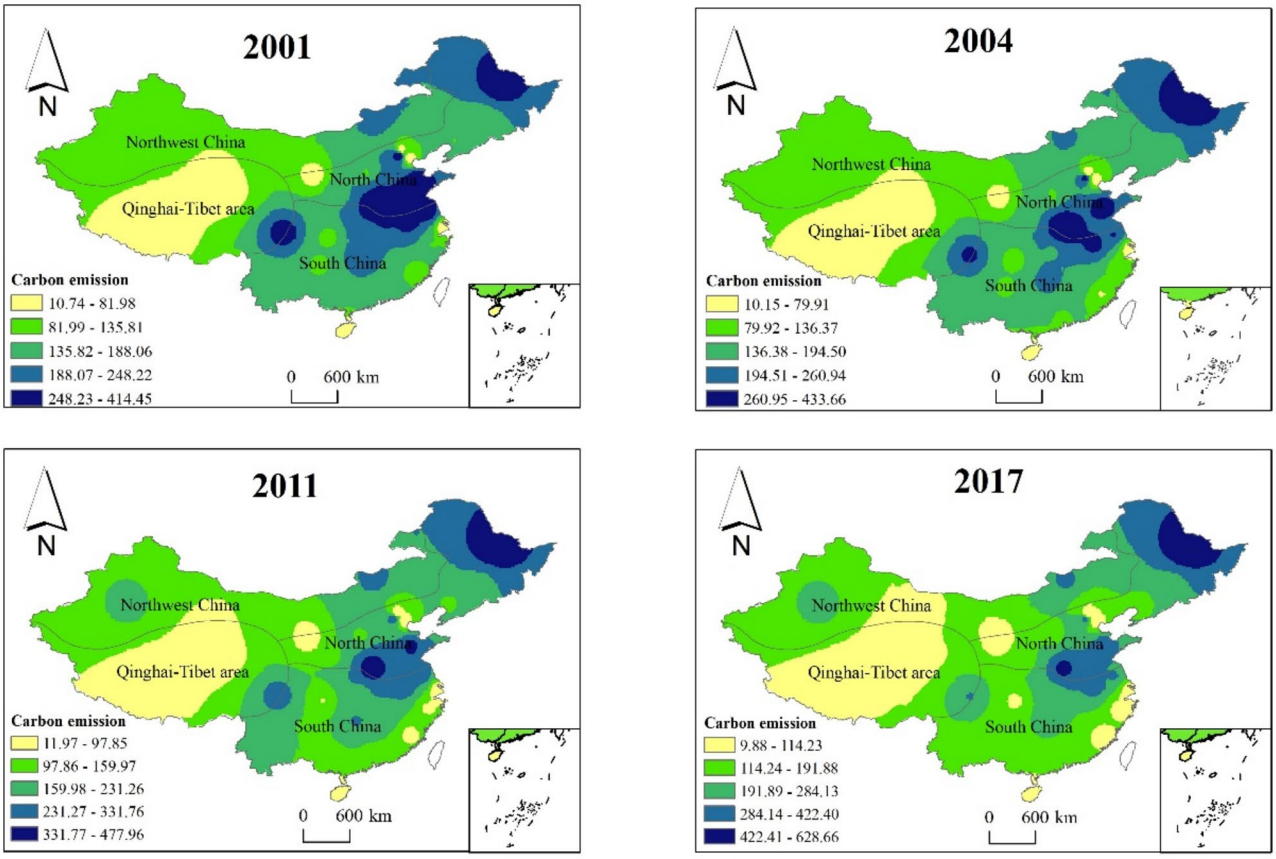

Fig. 7 Actual carbon emissions in drought (2001 and 2011) and wet years (2004 and 2017) across the sub-regions of China. (Million Tons)

South and North China have a higher proportion of land used for agriculture, industry, and urbanization, which reduces the area available for carbon sequestration and leads to higher carbon emissions [7].

Furthermore, a positive association was achieved across all sub-regions when we correlated the drought indices with carbon emissions in 2001 and 2011. The finding is logical in dry years; a positive correlation between carbon emissions and agricultural drought in dry years can harm photosynthesis, as drought stress can lead to abridged crop yield, changes in leaf physiology, changes in plant community arrangement, and changes in soil moisture, all of which can decrease rates of photosynthesis [21]. The results show a negative or lower correlation between soil moisture and carbon emissions in North China and Northwest China, while there is a Positive correlation in South China. A region's unique soil characteristics and environmental conditions can influence the interaction between soil moisture and carbon emissions. This is evident when comparing the regions of North, Northwest, and South China. The varied climates and soil types in these areas could be the reason behind the observed differences in correlations. A negative or lower correlation between soil moisture and carbon emissions is noted in North and Northwest China, whereas the correlation is positive in South China. This suggests that regional factors significantly affect the correlation between soil moisture and carbon emissions [28]. The semi-arid to arid conditions of North and Northwest China, characterized by limited and unsuitable rainfall, can stress soil moisture levels. This environmental stress can inhibit plant growth and negatively affect soil microbial activities. Such conditions may reduce carbon emission rates, as plant development and soil microbial roles are critical in the carbon cycle. This state highlights the exact impact of climatic factors on soil health and related carbon dynamics.

The incidence of alkaline soils in North and Northwest China, known for having lower organic matter content and diminished microbial activity, could also affect the lower carbon emissions examined in these regions. Alkaline soils often challenge microbial processes integral to the carbon cycle, leading to reduced decomposition and carbon release. This soil trait and the regional climatic conditions cause the unique carbon emission patterns in North and Northwest China [7]. With its ample and coherent rainfall, South China's subtropical to tropical climate typically results in higher soil moisture levels. This moist environment is promising

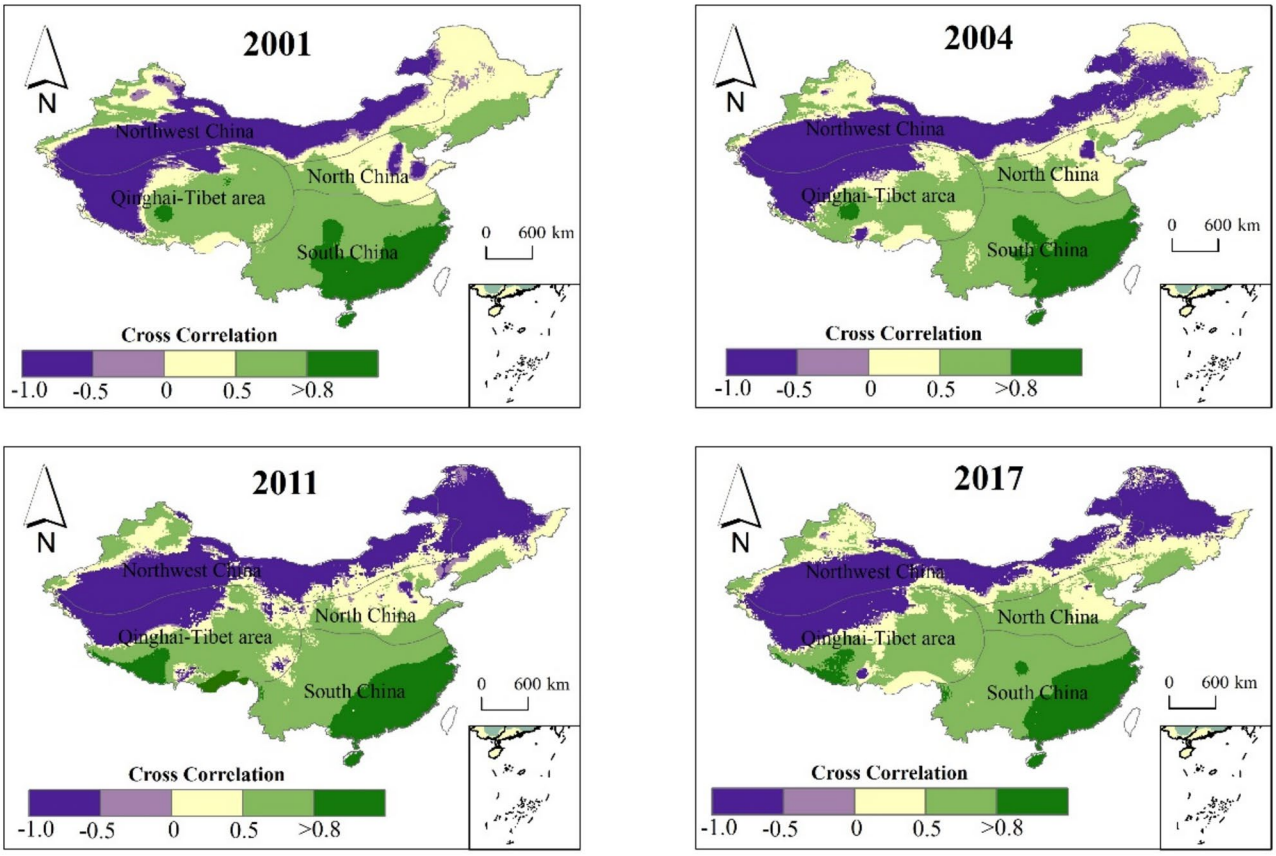

Fig. 8 Spatial cross-correlation between the carbon emissions and MAI

for robust plant growth and heightened soil microbial activity, which can hypothetically increase carbon emission rates. Furthermore, the superiority of acidic soils in South China, which are typically richer in organic matter and exhibit more significant microbial activity, might further enhance carbon emissions. The sequence of these climatic and soil conditions in South China creates an environment that contributes more to carbon release in North and Northwest China [40].

Moreover, a positive association between the VAI and carbon emissions was noted in South and North China and the Qinghai-Tibet region, while a negative relationship was monitored in Northwest China. The climatic conditions in South and North China, along with the Qinghai-Tibet area, typically more favorable to vegetation growth, such as higher rainfall and moderate temperatures, result in elevated VAI values and carbon emissions [28]. In contrast, the more severe climate of Northwest China, characterized by limited precipitation and extreme temperatures, tends to restrict vegetation growth and carbon emissions [32, 40]. Another factor causing this is the specific vegetation types in these regions. Forests and grasslands lead in South and North China and the Qinghai-Tibet area and are associated with higher carbon inclusion rates and emissions. However, desert vegetation, which is influential in Northwest China, is linked to lower carbon uptake rates and emissions [5, 7].

In South China, a positive correlation was found between carbon emissions and the (TAI), while in Northwest China and the northeastern part of North China, a negative correlation was noted during years of drought. Several factors could explain the differences in the correlation between carbon emissions and TAI in different regions of China during drought and wet years. One possible explanation is that South China is surrounded by the South China Sea and the East China Sea, which moderate temperatures [41, 42]. In contrast, Northwest China and northeast North China have a continental climate, which means they are far from moderating influences of large bodies of water. Inland regions often face extreme temperature fluctuations than coastal areas [25, 43, 44]. In winter, cold air masses from Siberia and Mongolia travel southward, causing particularly low temperatures in Northwest China and Northeast North China [30].

Additionally, variations in natural elements like vegetation cover and water availability across different regions can influence carbon dynamics. Areas experiencing

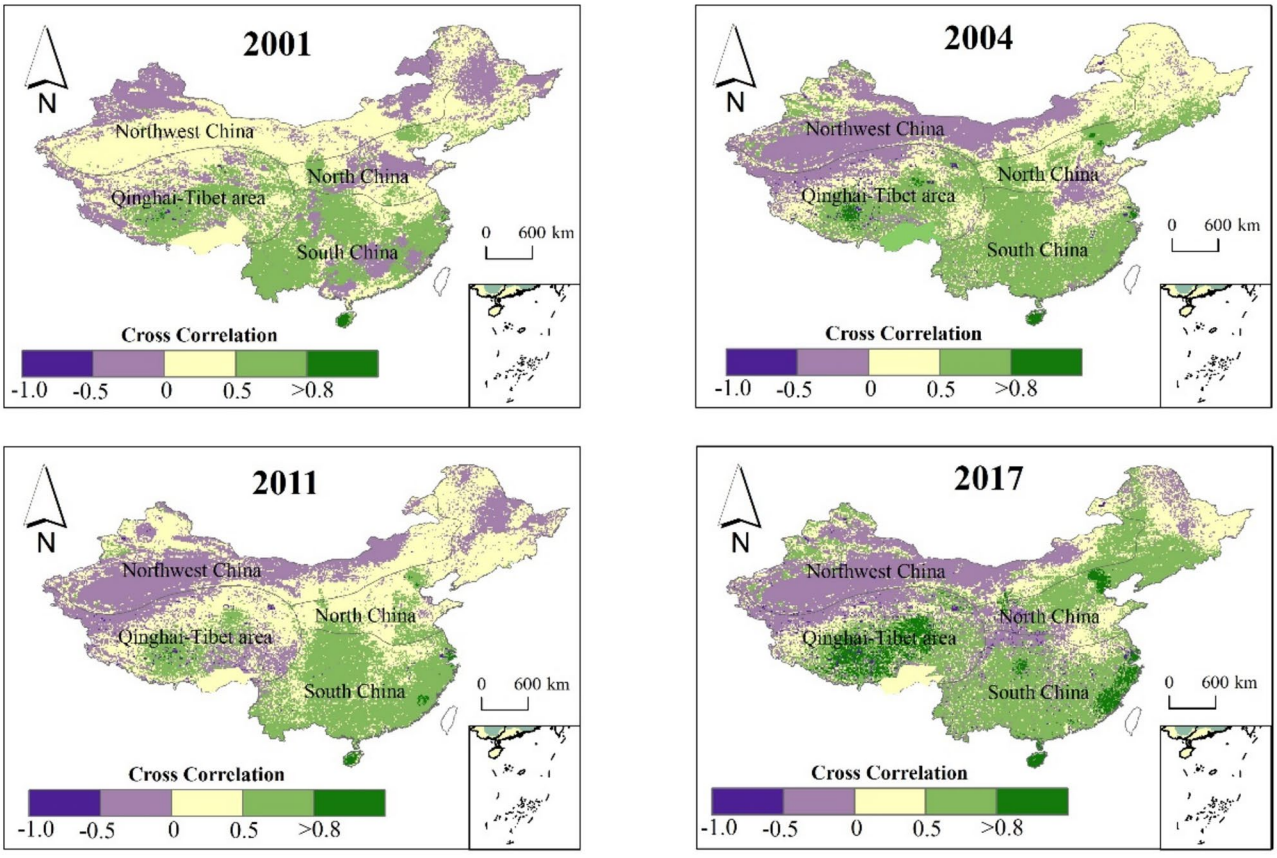

Fig. 9 Spatial cross-correlation between the carbon emissions and VAI

droughts, especially those with sparse vegetation or constrained water resources, might significantly impact carbon uptake and storage [16]. This can result in increased carbon emissions, as limited vegetation and water availability hinder the processes that typically sequester carbon [7, 28, 45]. Regions with more extensive vegetation coverage or better water availability will likely maintain their carbon sinks more effectively, even during drought [4, 46]. This capability to preserve carbon sinks is crucial in mitigating carbon emissions [31]. The presence of abundant vegetation facilitates the absorption and storage of carbon dioxide through photosynthesis [26]. Moreover, sufficient water availability supports this process, ensuring that plants remain healthy and function as effective carbon sinks. Consequently, these regions may exhibit lower carbon emission rates than areas with less vegetation or limited water resources, which struggle to sustain their carbon sequestration capacity under similar conditions.

Conclusions

This study highlights the critical role of agricultural drought monitoring in managing carbon emissions. Drought-induced changes in soil moisture and vegetation significantly impact the carbon cycle, reducing the ability of plants to sequester carbon and increasing atmospheric CO_2 levels. Additionally, drought conditions heighten plant vulnerability to diseases and pests, further impeding carbon absorption. Effective drought monitoring is essential for identifying stressed agricultural areas and mitigating rising carbon emissions through adaptive strategies such as improved irrigation and soil conservation practices. These proactive measures reinforce the importance of sustainable agriculture in addressing climate change.

From 2001 to 2020, this study assessed the impact of agricultural drought on carbon emissions across four distinct regions of China: Northwest China, North China, the Qinghai-Tibet region, and South China. By utilizing key indices, Moisture Anomaly Index (MAI), Vegetation Anomaly Index (VAI), and Temperature Anomaly Index (TAI), alongside statistical techniques such as auto-correlation and spatial cross-correlation analyses, the study explored the intricate relationship between drought indicators and carbon emissions.

The results revealed significant regional variations, with the VAI demonstrating the strongest correlation with carbon emissions. North China exhibited the

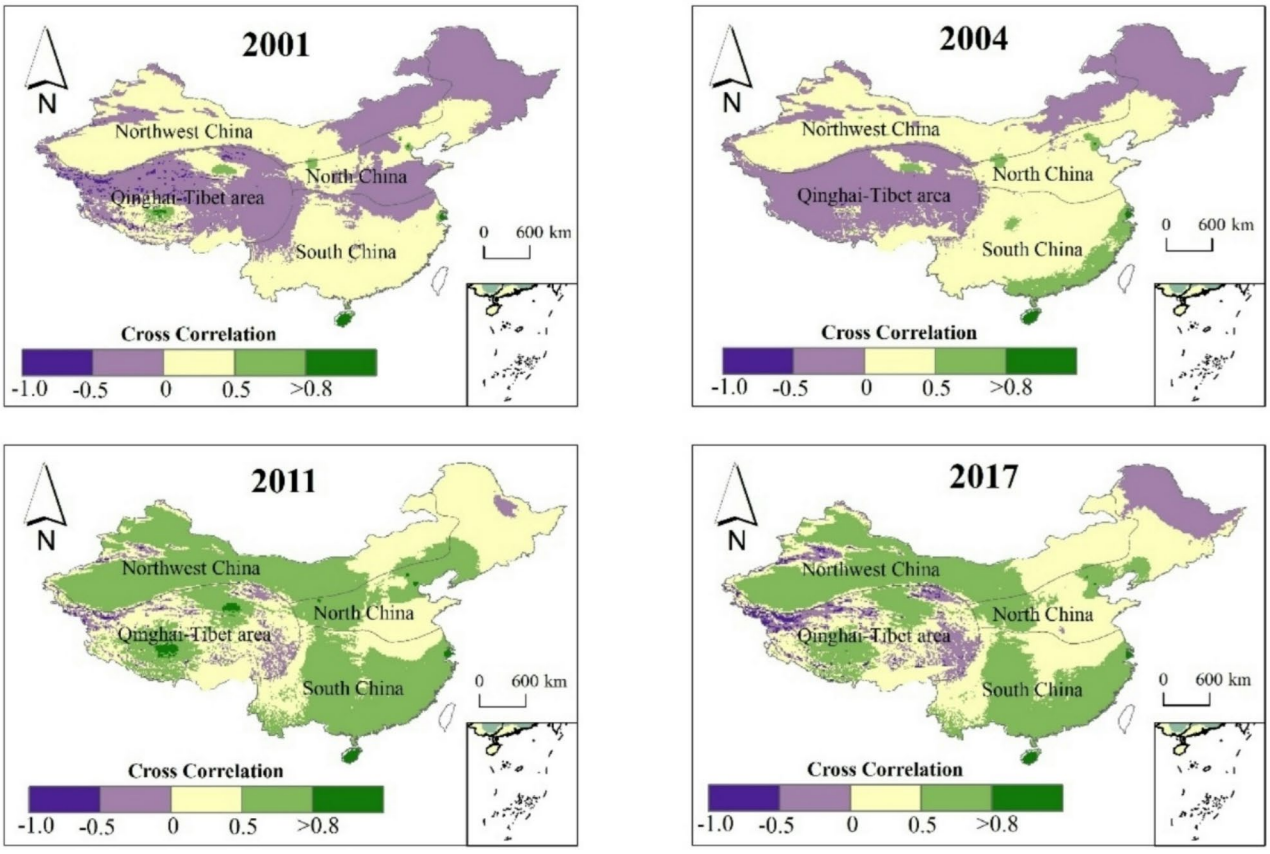

Fig. 10 Spatial cross-correlation between the carbon emissions and TAI

highest carbon emission levels, while spatial cross-correlation analysis indicated a positive correlation in South China and mixed correlations in other regions.

This study underscores the complex interplay between agricultural drought and carbon emissions, emphasizing the need for region-specific mitigation strategies. The insights gained contribute to climate change adaptation efforts and sustainable land management policies aimed at reducing the adverse effects of droughts on carbon emissions.

Acknowledgements
N/A.

Author contributions
Tehseen Javed and Zhenhua Wang: Conceptualization, Methodology, Software. Tehseen Javed, Jian Liu, Wenhao Li, and Haixia Lin1: Data curation, Writing - original draft preparation. Tehseen Javed: Visualization, Investigation Zhenhua Wang: Supervision. Pengpeng Chen, Jihong Zhang: Software, Validation. Tehseen Javed and Zhenhua Wang: Writing - reviewing and editing.

Funding
Funding support for this research was provided by the National Key R & D Project of China (No. 2022YFD1900405), the Third Xinjiang Scientific Expedition Program (No. 2022xjkk0500).

Data availability
No datasets were generated or analysed during the current study.

Declarations

Ethics approval and consent to participate
This study did not involve human participants or animals, so ethical approval was not required.

Consent to participate
This study did not involve human participants, so consent was not applicable.

Consent for publication
All authors have reviewed and approved the final version of the manuscript and consent to its submission and publication.

Competing interests
The authors declare no competing interests.

Received: 25 July 2024 / Accepted: 26 April 2025
Published online: 15 May 2025

References

1. Javed T, Yao N, Chen X, Suon S, Li Y. Drought evolution indicated by meteorological and remote-sensing drought indices under different land cover types in China. Environ Sci Pollut Res. 2020;27(4):4258–74.
2. Li K, Huang G, Wang S. Market-based stochastic optimization of water resources systems for improving drought resilience and economic efficiency in arid regions. J Clean Prod. 2019;233:522–37.
3. Yang Y, Yin J, Kang S, Slater LJ, Gu X, Volchak A. Quantifying the drivers of terrestrial drought and water stress impacts on carbon uptake in China. Agric for Meteorol. 2024;344:109817.

4. Zhao J, Liu Q, Lu H, Wang Z, Zhang K, Wang P. Future droughts in China using the standardized precipitation evapotranspiration index (SPEI) under multi-spatial scales. Nat Hazards. 2021;109(1):615–36.
5. Bhatti UA, Bhatti MA, Tang H, Syam M, Awwad EM, Sharaf M, et al. Global production patterns: Understanding the relationship between greenhouse gas emissions, agriculture greening and climate variability. Environ Res. 2024;245:118049.
6. Chen Y. A new methodology of Spatial cross-correlation analysis. PLoS ONE. 2015;10(5):e0126158.
7. Ding Y, Wang F, Mu Q, Sun Y, Cai H, Zhou Z, et al. Estimating land use/land cover change impacts on vegetation response to drought under 'grain for green'in the loess plateau. Land Degrad Dev. 2021;32(17):5083–98.
8. Didion-Gency M, Vitasse Y, Buchmann N, Gessler A, Gisler J, Schaub M, et al. Chronic warming and dry soils limit carbon uptake and growth despite a longer growing season in Beech and oak. Plant Physiol. 2024;194(2):741–57.
9. Henchiri M, Liu Q, Essifi B, Javed T, Zhang S, Bai Y, et al. Spatio-temporal patterns of drought and impact on vegetation in North and West Africa based on multi-satellite data. Remote Sens. 2020;12(23):3869.
10. Huang Y, Guo M, Bai P, Li J, Liu L, Tian W. Warming intensifies severe drought over China from 1980 to 2019. Int J Climatol.
11. Komuscu AU, Erkan A, Oz S. Possible impacts of climate change on soil moisture availability in the Southeast Anatolia development project region (GAP): an analysis from an agricultural drought perspective. Clim Change. 1998;40(3):519–45.
12. Yang F, Duan X, Guo Q, Lu S, Hsu K. The Spatiotemporal variations and propagation of droughts in plateau mountains of China. Sci Total Environ. 2022;805:150257.
13. Javed T, Li Y, Rashid S, Li F, Hu Q, Feng H, et al. Performance and relationship of four different agricultural drought indices for drought monitoring in China's Mainland using remote sensing data. Sci Total Environ. 2021;759:143530.
14. Javed T, Wang Z, Liu J, Li W, Lin H, Zhang J. Unlocking the ecohydrological dynamics of vegetation growth's impact on terrestrial water storage trends across the China-Pakistan economic corridor. Sci Total Environ. 2024;955:176977.
15. Van der Molen MK, Dolman AJ, Ciais P, Eglin T, Gobron N, Law BE, et al. Drought and ecosystem carbon cycling. Agric for Meteorol. 2011;151(7):765–73.
16. Wang F, Lai H, Li Y, Feng K, Zhang Z, Tian Q, et al. Dynamic variation of meteorological drought and its relationships with agricultural drought across China. Agric Water Manage. 2022;261:107301.
17. Grillakis MG. Increase in severe and extreme soil moisture droughts for Europe under climate change. Sci Total Environ. 2019;660:1245–55.
18. Kamangar M, Kisi O, Minaei M. Spatio-Temporal analysis of carbon sequestration in different ecosystems of Iran and its relationship with agricultural droughts. Sustainability. 2023;15(8):6577.
19. Liu Y, Zhou Y, Ju W, Wang S, Wu X, He M, et al. Impacts of droughts on carbon sequestration by China's terrestrial ecosystems from 2000 to 2011. Biogeosciences. 2014;11(10):2583–99.
20. Yao Z, Zhang W, Wang X, Lu M, Chadwick D, Zhang Z, et al. Carbon footprint of maize production in tropical/subtropical region: a case study of Southwest China. Environ Sci Pollut Res. 2021;28(22):28680–91.
21. Katsnelson MI. Carbon in two dimensions. UK: Cambridge University Press Cambridge; 2012.
22. Dye AW, Houtman RM, Gao P, Anderegg WR, Fettig CJ, Hicke JA, et al. Carbon, climate, and natural disturbance: a review of mechanisms, challenges, and tools for Understanding forest carbon stability in an uncertain future. Carbon Balance Manag. 2024;19(1):35.
23. Guidolotti G, Zenone T, Endreny T, Pace R, Ciolfi M, Mattioni M, et al. Impact of drought on cooling capacity and carbon sequestration in urban green area. Urban Clim. 2025;59:102244.
24. Grossiord C, Bachofen C, Gisler J, Mas E, Vitasse Y, Didion-Gency M. Warming May extend tree growing seasons and compensate for reduced carbon uptake during dry periods. J Ecol. 2022;110(7):1575–89.
25. Yang J, Huang Y, Takeuchi K. Does drought increase carbon emissions? Evidence from Southwestern China. Ecol Econ. 2022;201:107564.
26. Ma L, Qiao C, Du L, Tang E, Wu H, Shi G, et al. Drought in the middle growing season inhibited carbon uptake more critical in an anthropogenic shrub ecosystem of Northwest China. Agric for Meteorol. 2024;353:110060.
27. Wolf S, Paul-Limoges E. Drought and heat reduce forest carbon uptake. Nat Commun. 2023;14(1):6217.
28. Cui Y, Khan SU, Deng Y, Zhao M. Spatiotemporal heterogeneity, convergence and its impact factors: perspective of carbon emission intensity and carbon emission per capita considering carbon sink effect. Environ Impact Assess Rev. 2022;92:106699.
29. Chen X, Li Y, Yao N, Liu DL, Liu Q, Song X et al. (2022). Projected dry/wet regimes in China using SPEI under four SSP-RCPs based on statistically downscaled CMIP6 data. Int J Climatol.
30. Javed T, Zhang J, Bhattarai N, Sha Z, Rashid S, Yun B, et al. Drought characterization across agricultural regions of China using standardized precipitation and vegetation water supply indices. J Clean Prod. 2021;313:127866.
31. Li C, Filho L, Yin W, Hu J, Wang R, Yang J, C., et al. Assessing vegetation response to multi-time-scale drought across inner Mongolia plateau. J Clean Prod. 2018;179:210–6.
32. Zhou Z, Shi H, Fu Q, Li T, Gan TY, Liu S. Assessing Spatiotemporal characteristics of drought and its effects on climate-induced yield of maize in Northeast China. J Hydrol. 2020;588:125097.
33. Amri R, Zribi M, Lili-Chabaane Z, Duchemin B, Gruhier C, Chehbouni A. Analysis of vegetation behavior in a North African semi-arid region, using SPOT-VEGETATION NDVI data. Remote Sens. 2011;3(12):2568–90.
34. Loeb GE, White MW, Merzenich MM. Spatial cross-correlation. Biol Cybern. 1983;47(3):149–63.
35. Gudmundsson L, Tallaksen LM, Stahl K. Spatial cross-correlation patterns of European low, mean and high flows. Hydrol Process. 2011;25(7):1034–45.
36. Meza I, Rezaei EE, Siebert S, Ghazaryan G, Nouri H, Dubovyk O, et al. Drought risk for agricultural systems in South Africa: drivers, Spatial patterns, and implications for drought risk management. Sci Total Environ. 2021;799:149505.
37. Zhang J, Mu Q, Huang J. Assessing the remotely sensed drought severity index for agricultural drought monitoring and impact analysis in North China. Ecol Ind. 2016;63:296–309.
38. Kim YS. Construction and operation of the National landslide forecast system using soil water index in Republic of Korea. J Korean Soc Hazard Mitigation. 2015;15(6):213–21.
39. Matlou R, Bahta YT, Owusu-Sekyere E, Jordaan H. Impact of agricultural drought resilience on the welfare of smallholder livestock farming households in the Northern cape Province of South Africa. Land. 2021;10(6):562.
40. Liu X, Zhu X, Pan Y, Li S, Liu Y, Ma Y. Agricultural drought monitoring: progress, challenges, and prospects. J Geog Sci. 2016;26(6):750–67.
41. Poonia V, Goyal MK, Gupta B, Gupta AK, Jha S, Das J. Drought occurrence in different river basins of India and blockchain technology based framework for disaster management. J Clean Prod. 2021;312:127737.
42. Wang Z, Li J, Lai C, Zeng Z, Zhong R, Chen X, et al. Does drought in China show a significant decreasing trend from 1961 to 2009? Sci Total Environ. 2017;579:314–24.
43. Łabędzki L, Bąk B. (2014). Meteorological and agricultural drought indices used in drought monitoring in Poland: a review. Meteorol Hydrology Water Manage Res Oper Appl, *2*.
44. Wei Y, Ru H, Leng X, He Z, Ayantobo OO, Javed T, et al. Better performance of the modified CERES-Wheat model in simulating evapotranspiration and wheat growth under water stress conditions. Agriculture. 2022;12(11):1902.
45. Boken VK, Cracknell AP, Heathcote RL. Monitoring and predicting agricultural drought: a global study. Oxford University Press; 2005.
46. Yang Y, Gan TY, Tan X. Spatiotemporal changes of drought characteristics and their dynamic drivers in Canada. Atmos Res. 2020;232:104695.

Publisher's note